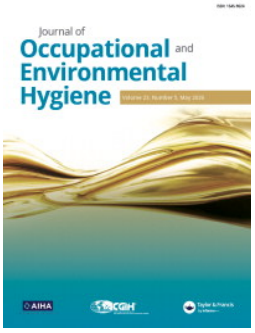

Taylor & Francis
Taylor & Francis Group

Journal of Occupational and Environmental Hygiene

ISSN: 1545-9624 (Print) 1545-9632 (Online) Journal homepage: www.tandfonline.com/journals/uoeh20

Mathematical optimization of filters used in N95 filtering facepiece respirators

Patrick T. O'Shaughnessy

JOURNAL OF OCCUPATIONAL AND ENVIRONMENTAL HYGIENE
https://doi.org/10.1080/15459624.2026.2659853

Mathematical optimization of filters used in N95 filtering facepiece respirators

Patrick T. O'Shaughnessy

Department of Occupational and Environmental Health, The University of Iowa, Iowa City, Iowa

ABSTRACT

The filter used in an N95 filtering facepiece respirator (FFR) has a collection efficiency and pressure drop that are primarily influenced by filter depth and solidity, as well as the average diameter and electrostatic charge of its fibers. A sensitivity analysis was performed to determine the influence of each property on particle collection efficiency at the most penetrating particle size (MPPS) and pressure drop using previously verified N95 FFR filter performance models. Collection efficiency was most influenced by changes in filter solidity and least influenced by fiber charge. Likewise, pressure drop was most influenced by fiber diameter, least influenced by changes in filter depth, and was not affected by fiber charge. Given the competing desire for low pressure drop and high collection efficiency, the use of a quality factor demonstrated that increasing filter charge and fiber diameter had a nearly equal positive association with overall filter efficacy. A filter optimization process was also conducted that employed a non-linear optimization routine to first determine the filter depth required to obtain a collection efficiency criterion of $\geq$ 95% collection efficiency at the MPPS for sets of fiber diameter and filter solidity values, and to determine the pressure drop resulting from each combination of the three property values while holding fiber charge constant. This analysis demonstrated that filters with low solidity, high fiber diameter, and high depth produce the lowest pressure drop. However, all combinations of filter properties within the ranges analyzed produced acceptable pressure drops, indicating that an upper limit on filter depth can be applied based on N95 FFR design constraints and still maintain a reasonable pressure drop. To aid filter design efforts, linear regression models were developed to first predict the filter depth needed to meet the efficiency criterion given known fiber diameter and filter solidity, and then to predict the pressure drop from those three properties.

KEYWORDS

Efficiency; FFR; MPPS; pressure drop; quality factor

Introduction

Respirators are a common form of personal protective equipment used to reduce exposure to harmful air contaminants in the workplace. Filtering facepiece respirators (FFRs) are a class of respirators that includes the N95-designated respirator, designed to reduce exposures to airborne particulate matter in scenarios that contain dry aerosols and cannot otherwise be controlled to reduce aerosol concentrations. FFRs are approved by NIOSH using a specified procedure (NIOSH 2019b) in which the penetration of a sodium chloride aerosol through a sealed N95 FFR is assessed. The collection efficiency of 20 representative FFRs of the type to be tested must be $\geq$ 95% when subjected to a consistent inflow rate of 85 L/min to pass the test.

While designing N95 FFR filter media to meet the efficiency-passing criteria, manufacturers must also consider the pressure drop developed by the filter media. An N95 FFR cannot produce a pressure drop greater than 35 mm H_2O at 85 L/min of inflowing air (NIOSH 2019a). Respirators must obtain a relatively high collection efficiency together with a low filter pressure drop, which is the primary design concern when developing filter media used in FFRs. However, there are few scientific investigations of the primary properties of N95 filter media (both fiber and filter characteristics) and their individual influences on both particle capture efficiency, E, and pressure drop (Δp) in the literature. The studies by Chen et al. (1993) and Huang et al. (2013) are two of the few studies

CONTACT Patrick T. O'Shaughnessy patrick-oshaughnessy@uiowa.edu Department of Occupational and Environmental Health, The University of Iowa, Iowa City, IA 52241.

Supplemental data for this article can be accessed online at https://doi.org/10.1080/15459624.2026.2659853. AIHA and ACGIH members may also access supplementary material at http://oeh.tandfonline.com.

that systematically altered a variety of filter media properties to identify their effect on filter efficiency and pressure drop. Whereas many other papers have described the combined effects of filter properties to determine FFR performance under various conditions, such as changes in face velocity (Balazy et al. 2006), changes in relative humidity (Ramirez and O'Shaughnessy 2016), and fiber charge levels (Barrett and Rousseau 1998), they did not isolate the individual effects of filter properties.

Filter optimization (attaining the highest efficiency with the lowest pressure drop) can be enhanced if the individual influence of each filter and fiber property on both *E* and Δp is known. The important properties of the fibers include their diameter and amount of electrostatic charge. Likewise, the influential properties of the entire filter include its depth (thickness) and solidity (packing density). Filter solidity is the ratio of the volume of all fibers to the volume of the filter (Hinds 1999) and is therefore the direct opposite of the filter's porosity. Factors external to the filter can also affect its *E* and Δp. They include the density and the charge state of the aerosol particle being captured that directly affect *E*. Likewise, the rate of inflowing air, which influences the velocity of the inhaled air through the filter, affects both *E* and Δp.

Theoretical equations have been developed to estimate the *E* of particulate filters based on their properties (Davies 1973; Brown 1993; Hinds 1999). These equations determine the filtration of particles by simulating the effects of the forces of interception, impaction, diffusion, gravitational settling, and electrostatic attraction. With the use of equations to simulate these collection mechanisms based on the properties of single filter fibers, the total collection efficiency of a filter can be determined based on its depth and solidity. Two related papers by this research group provide a thorough explanation of these capture efficiency equations (O'Shaughnessy 2022) and refine their attributes to maximize their ability to simulate the capture efficiency of currently available N95 FFRs (O'Shaughnessy et al. 2023).

Although papers have recently been published that report on optimized filter production processes (Niu et al. 2021; Kamil and Munir 2023), few have been written that attempt to optimize the magnitude of filter properties relative to the competing interests of low pressure drop and high efficiency. Of those, Pradhan et al. (2016) employed a three-component lattice design, each with a different blend of coarse and fine fibers, to test and compare for efficiency and pressure drop. With equations from experimental data, they were able to develop contour plots within the triangular space of the lattice design that showed gradations of filtration efficiency and another for pressure drop. Ptak (1993) also explored the use of optimization procedures for enhancing filter performance but focused on the use of simple criterion functions, including the "quality factor" (QF) described in texts (Brown 1993; Hinds 1999), which combines the competing effects of *E* and pressure drop Δp, where a filter that produces a higher QF is considered advantageous:

$$QF = \frac{-\ln(1-E)}{\Delta p} \quad (1)$$

Ptak (1993) also suggested other criteria, such as a simpler form of QF, Q' = $E/\Delta p$, and a differencing criterion, Q" = λ_1 *E* – $\lambda_2 \Delta p$, where the weights λ_1 and λ_2 can be given the same value (0.5) or different values depending on which filter quality is of most importance.

The primary objective of this study was to perform numerical simulations focused on the optimization of an N95 FFR to determine the characteristics of filter properties that result in minimizing pressure drop while maintaining a particle capture efficiency criterion of $E \geq 95\%$ at the most penetrating particle size (MPPS). Optimization steps involved adjusting filter solidity and average fiber diameter values, and using an optimization routine to obtain a filter depth that meets the efficiency criterion while holding air flow rate and electrostatic charge constant. A sensitivity analysis was also performed to determine which physical properties had the greatest effect on *E* and Δp.

Methods

Efficiency and pressure drop models

The particle capture efficiency model used in this study is fully described in O'Shaughnessy (2022). The efficiency model was developed using theoretical models from a variety of sources to simulate single-fiber collection efficiency using equations for the following forces: diffusion (Wang et al. 2007), interception (Lee and Liu 1982), impaction and gravitation (Stechkina et al. 1969), and fiber charge (Lathrache and Fissan 1987). These equations were applied as described in their respective papers, except for the diffusion equation. Wang et al. (2007) suggested that the diffusion force, E_D, can be described by the power law. $E_D = b \cdot Pe^m$, where *Pe* is the Peclet number. Values for the constant ($b = 0.19$) and exponent ($m = -0.42$) were empirically determined by O'Shaughnessy et al. (2023)

to best represent the effect of the diffusion force associated with the filtering layer of a typical N95 filter by maximizing the correlation between model output and measurements of N95 FFR filter efficiencies over a range of particle sizes. From the sum of all single-fiber efficiency equations (E_s), total filter layer efficiency (E) was computed using Equation 2 (Lathrache and Fissan 1987):

$$E = 1 - \exp\left[\frac{-4\alpha E_s L}{\pi d_f(1-\alpha)}\right] \tag{2}$$

where α is the solidity of the filter, L is the filter depth, and d_f is the average fiber diameter.

The aerosol applied to the model was assumed to be sodium chloride with a density of 2.16 g/cm^3 and the dielectric constant of 5.9. Equations were added to the model to compute the charge per particle diameter assuming a Boltzmann equilibrium charge distribution, which develops on aerosols given sufficient time to reach this equilibrium state (Lathrache and Fissan 1987; Chen et al. 1993). The properties of the simulated conditions included an air temperature of 20 °C flowing with a face velocity through the N95 FFR of 8 cm/s that was similar to the face velocity of a typical N95 with a surface area of 175 cm^2 subjected to an inward flow rate of 85 L/min (O'Shaughnessy et al. 2021). Likewise, the filter fibers were assumed to be 100% polypropylene that had a dielectric constant of 2.2. A reproduction of a plot from O'Shaughnessy et al. (2023) showing the relationship between measured efficiency and the best-fit model curve is provided in Figure S1 of the Supplement.

The equation for Δp used in this work was originally developed by Davies (1953):

$$\Delta p = \frac{\mu L U_0 f(\alpha)}{d_f^2} \tag{3}$$

where μ is the fluid viscosity, and U_o is the face velocity. The original function (f(α)) of Equation 3, given by Davies, was modified by O'Shaughnessy et al. (2023) by changing the leading constant from 64 to 8.3, as shown in Equation 4, to cause Equation 3 to best represent the pressure drop across a typical N95 FFR:

$$f(\alpha) = 8.3\alpha^{1.5}(1 + 56\alpha^3). \tag{4}$$

The E and Δp models were developed in a Microsoft Excel Version 2503 spreadsheet. The E model was designed to calculate filter efficiency across 31 particle diameters evenly spaced (ten per decade) on a log scale over the range of 0.001–1 μm.

Note that a typical N95 FFR consists of three layers: outer, filtering, and inner. The outer layer is composed of stiff fibrous material required to support the shape of the FFR, whereas the inner layer is composed of finer material that provides a comfortable feeling against the skin. Both the inner and outer layers are designed to minimize additional pressure drop and therefore do not add substantially to E. The middle "filtering" layer is composed of charged nonwoven fibrous strands that serve as the primary means of particle capture by the FFR. The E and Δp models were developed to best simulate the performance of the filtering layer under the simplifying assumption that if the optimization process results in the filtering layer meeting the NIOSH approval criteria, then a multi-layer FFR is bound to meet the criteria. A comparison of the efficiency and pressure drop of a three-layer FFR (Model 8510, 3 M Corp., St. Paul, MN) relative to the filtering layer was conducted to justify this assumption. The properties of those additional layers are described in Ramirez and O'Shaughnessy (2016).

As described in O'Shaughnessy et al. (2023), measurements of the filtering layer from six N95 FFRs were obtained to compute average values of filter depth (0.12 cm), the average fiber diameter (or effective diameter) of their distribution of diameters (2.5 μm), and solidity (0.085) of the filtering layer, which were used in this study to represent those of a typical N95 FFR. Likewise, they performed a literature search to determine a typical charge per fiber area of 23.5 μC/m^2. When applied to the E model, these values produced an efficiency curve relative to particle diameter that is like that of most N95 FFRs, with a minimum efficiency of 96.4% and a most penetrating particle size (MPPS) of 0.039 μm. Likewise, the Δp model produced a filter pressure drop of 6.1 mm H_2O under these conditions, which was reasonably close to the average of measured Δp for the six N95 FFRs of 6.2 mm H_2O.

Sensitivity analysis

A sensitivity analysis was conducted that involved changing the magnitude of each of four fiber and filter properties (fiber diameter and charge; filter solidity and depth) over a range of their values (Table 1). To facilitate comparisons between properties, the range of each was established by using the typical value as the middle value of each range with three evenly spaced values above and below the middle, and with lowest and highest values that were 50% and 150%,

Table 1. Range of values of filter properties applied to the efficiency and pressure drop models.

	Filter Solidity	Filter Depth cm	Fiber Diameter μm	Fiber Charge μC/m^2
Minimum	0.043	0.06	1.25	11.8
Middle	0.085	0.12	2.50	23.5
Maximum	0.128	0.18	3.75	35.3

respectively, of the middle value. This construct produced seven values for each property such that the highest value was threefold higher than the lowest value.

As will be demonstrated in the Results section, most properties caused nonlinear changes in either E or Δp with changes in their values. Therefore, a sensitivity analysis was performed by determining the difference in responses of an outcome resulting from application of the minimum and maximum property value to a model, given that each property was evaluated over the same proportional range (3x) of values. The sensitivities of E and Δp to small, nearly linear changes near the property values associated with a typical N95 FFR were also assessed after making 1% changes in the property values.

Although not a property of the filter, the inspiration flow rate, and, therefore, the face velocity of air through the filter (U_o) has been shown to affect both efficiency and pressure drop (Huang et al. 2013; O'Shaughnessy et al. 2023). The filter model was therefore also used to determine the effect of varying inspiration flow rates during sinusoidal breathing with a minute volume of 85 L/min. A minute volume of that magnitude can be considered "heavy breathing," for which a high breathing rate of 30/min was chosen, resulting in 2.8 L/breath (Janssen et al. 2005). As shown in Figure S2, the inspired flow rates over the 1s inspiration increased above 85 L/min after 0.1 s and reached a maximum of 267 L/min, which is equivalent to $U_o = 25.6$ cm/s for an FFR surface area of 175 cm^2. Figure S2 was created while applying the simplifying assumption that human breathing is sinusoidal, whereas actual breathing patterns exhibit steeper rises and falls during a breath (Napoli et al. 2022).

Filter optimization

Filter optimization was conducted in an unconstrained and a constrained manner. Unconstrained optimization was conducted with the use of Equation 1 to calculate the QF during which each of the four properties was adjusted from their minimum to maximum value as given in Table 1, while the other three properties were held constant at their typical value. To compute QF, the value of E applied to Equation 1 was the minimum efficiency associated with the efficiency of the MPPS.

Given the focus of this study on the performance of filters applied to N95 FFRs, a second optimization analysis was performed in which E was constrained to $\geq$ 95% at the MPPS as the success criterion. Note, however, that the NIOSH test (NIOSH 2019b) does not involve N95 FFR approval based on this criterion. Rather, that test provides a single efficiency across all particle sizes of the aerosol detected by a photometer that cannot discriminate by particle size. Since the optimization model used here involved calculations of efficiency across a wide range of particle diameters, constraining the efficiency at the MPPS to $\geq$ 95% was applied as a conservative measure of filter performance. An analysis was also conducted to demonstrate that a filter meeting this criterion will necessarily pass the less restrictive NIOSH approval process.

To initiate this analysis, the total combination of all four properties, each having seven values, potentially applied to the E model was reduced from all possible combinations ($n = 2{,}401$) in two ways. First, the assumption was made that a manufacturer of filter media would be able to control both the fiber diameter and filter solidity during the production process. Likewise, by theory, the fiber charge did not affect the pressure drop because it did not alter the structure of the filter. Therefore, the optimization process proceeded by systematically varying both the fiber diameter and filter solidity through their 49 (7×7) combinations while solving for the filter depth that satisfied the efficiency criterion, while the fiber charge remained fixed at its typical value of 23.5 μC/m^2 and with an inflowing air velocity of 8 cm/s.

The non-linear optimization code (Solver) in Microsoft Excel was used to perform the optimization process. Before using Solver, the MIN() function was added to a cell to find the minimum efficiency across all collection efficiencies calculated at each of the 31 particle diameters by the E model. One of the 49 possible combinations of fiber diameter and filter solidity values was added to cells in the optimization. The Solver function was opened to display the "Solver Parameters" window. The default Generalized Reduced Gradient (GRG) Nonlinear solving method was chosen (Fylstra et al. 1998). The default options of the GRG method, such as a constraint precision of 0.000001 and convergence of 0.0001, were also used. The cell containing the filter depth value was chosen as the "Set Objective." Options in the window were then chosen to minimize the value of the objective cell while also using that cell as the "Changing Variable Cell." Solver found a solution by adding the constraint that the cell containing the MIN() function must be $\geq$ 0.95. Using the Solver routine, therefore, resulted in the lowest filter depth, which, as a consequence, resulted in the lowest Δp for a set of fiber diameter and filter solidity values while also meeting the efficiency criterion. This process was repeated for all other fiber diameter and filter solidity combinations.

To facilitate filter design efforts, two general linear models (GLMs) were developed from the optimization output. A GLM was developed to predict the filter depth needed to meet the efficiency criterion with fiber diameter and solidity as the independent variables. A second GLM was then developed to predict the pressure drop resulting from the combination of the three filter properties: fiber diameter, solidity, and filter depth at a fixed fiber charge level of 23.5 $\mu C/m^2$ and inflow face velocity of 8 cm/s.

Results and discussion

Model output

An example of model output after applying all property values at their typical (middle) level is given in Figure 1, in which the total efficiency, *E*, of the filtering layer of an N95 FFR is shown relative to particle diameter (Table 1). The *E* curve shown in Figure 1 demonstrates the "dip" in efficiency caused by the reduction in the diffusion force and the increase in the charge (dielectrophoretic) force with increasing particle diameter, which caused the MPPS to fall between the particle diameters of 0.03 and 0.05 μm (O'Shaughnessy 2022).

Also shown in Figure 1 is the total efficiency curve developed when the three layers of a typical N95 FFR were considered. Model simulations together with photomicrographs of the fibers in each layer are given in Figure S3. The addition of the two layers only increased *E* from 96.4% to 97.2%, primarily because they do not consist of charged fibers. Likewise, there was only a slight increase in pressure drop from 6.06 mm H_2O to 6.32 mm H_2O due to their low solidity.

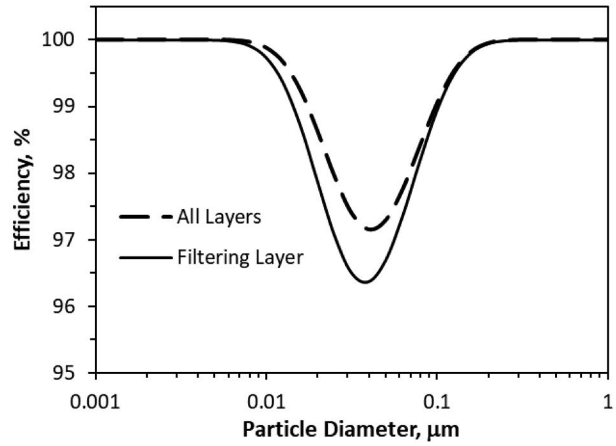

Figure 1. Efficiency model results for the single filtering layer and for an N95 consisting of two additional layers.

Sensitivity analysis

The sensitivity of each outcome to minimum *E* and Δp over their three-fold range is displayed and enumerated in Figure 2. As shown in Figure 2A, the effect of fiber charge across its range was smaller than the nearly equal effect of the other three properties on minimum efficiency. Fiber diameter is the only property that oppositely affected both outcomes—a larger diameter resulted in a lower outcome value and hence the negative difference (−21.5 mm H_2O) associated with that property as shown in Figure 2A.

Furthermore, Figure 2B demonstrates the counterintuitive finding that changes in filter depth did not affect Δp as much as changes in fiber diameter over their respective three-fold ranges. However, as shown in Equation 3, Δp is directly proportional to filter depth but is inversely proportional to the square of fiber diameter, which markedly increases the effect of fiber diameter on Δp. Note also from Figure 2B that fiber charge did not affect pressure drop since changes in that property did not result in structural changes that influenced Δp.

The related curves developed across the range of all seven property values applied for filter depth, filter solidity, fiber diameter, and fiber charge are shown in Figures S4–S7, respectively. The lower effect of fiber charge on minimum efficiency across its range is shown in Figure S7A relative to that of the other properties (Figures S4A, S5A, and S6A). However, the advantage of applying a charge to filter fibers can be seen in Figure S7C, where an additional charge level at 0.0 $\mu C/m^2$ was plotted. With no charge applied, the minimum efficiency dropped to 59% (for the same depth, solidity, and fiber diameter). However, applying a fiber charge as low as 11.8 $\mu C/m^2$ considerably increased the minimum efficiency to 91.3%. Relatively

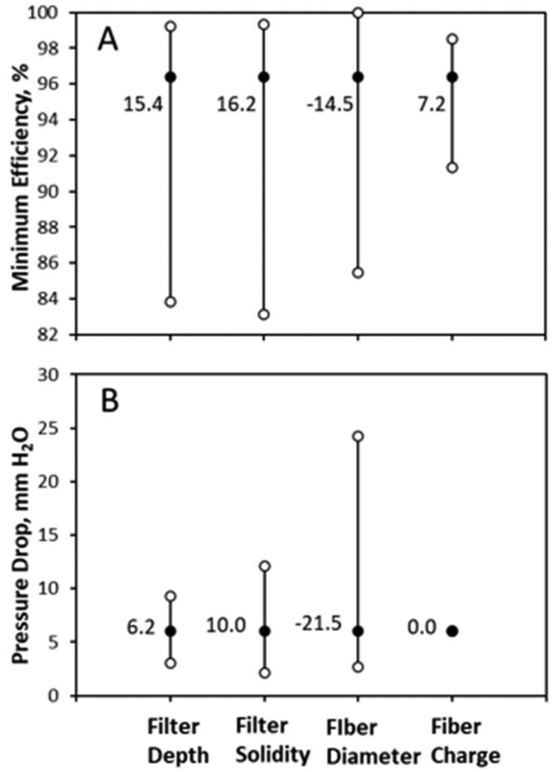

Figure 2. Changes in minimum efficiency (A) and pressure drop (B) for each property at their minimum and maximum values applied to the model. Black circles (•) indicate the outcome value for the middle value of the range analyzed. Values in plot A indicate the difference in minimum percent efficiency, and the values in plot B indicate the difference in mm H_2O.

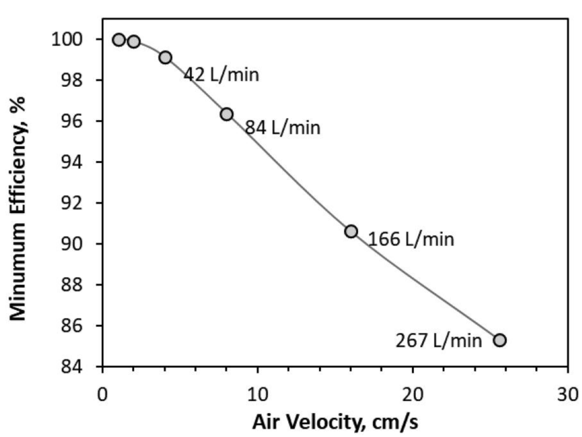

Figure 3. Plot demonstrating the effect of increases in air velocity on the filter minimum efficiency at the most penetrating particle size. The corresponding inflow rates at each air velocity evaluated are also shown.

less additional gain in minimum efficiency was then achieved by increasing this force as the fiber charge per area tended toward a maximum possible. Figure S7C and D also reveal that changes in filter charge had a large effect on the MPPS, which shifted from 0.15 µm with no charge to 0.03 µm at the highest charge value applied. This effect resulted from filtration relying on interception when no charge force was applied, which also increased with increasing particle diameter, but did not influence the capture of smaller particles to the extent of fiber charge. Reliance on interception to establish the right side of the efficiency dip, therefore, results in the MPPS being shifted to larger diameter particles (O'Shaughnessy 2022).

Table 2. Percent changes in filter efficiency and pressure drop relative to a 1% change in the typical property value.

Property	Change in Efficiency, %	Change in Pressure Drop, %
Depth	0.11	1.01
Diameter	−0.17	−1.98
Solidity	0.12	1.61
Charge	0.07	0.00

The effect of 1% changes from the typical property values is given in Table 2. In general, those changes had a much greater impact (approximately 1%) on pressure drop than on collection efficiency (approximately 0.1%). Furthermore, as demonstrated in the previous analysis, changes in fiber diameter had the most influence on both efficiency and pressure drop.

The effect of changes in inspiration flow rate while breathing with a minute volume of 85 L/min is given in Figure 3. The very low flow rates and related velocities at the start of a breath resulted in nearly 100% capture efficiency. However, as flow rates increased from 42 L/min (4 cm/s) to the peak of 267 L/min (25.6 cm/s), a nearly linear decrease in efficiency was achieved. This effect is caused by a reduction in both the diffusion and dielectrophoretic charge forces as velocity increases, which are most influential in creating the efficiency dip of the dielectric filters used in N95 FFRs (O'Shaughnessy et al. 2021).

Unconstrained filter property optimization

A comparison of the effect of each filter and fiber property on QF is given in Figure 4. A range of values was applied to each property such that they consisted of the same proportional differences from the middle (typical) value and extended from 0.5 to 1.5 times the middle value. Therefore, to enable a direct comparison of the influence of changes in each property, the QF values are displayed in Figure 4 in relation to the fraction of each range value relative to the middle value for each property. Given that the middle value of each range is also the declared typical value and is applied for each property while all other properties were held at their typical value, the minimum efficiency and pressure drop values are the same for each middle

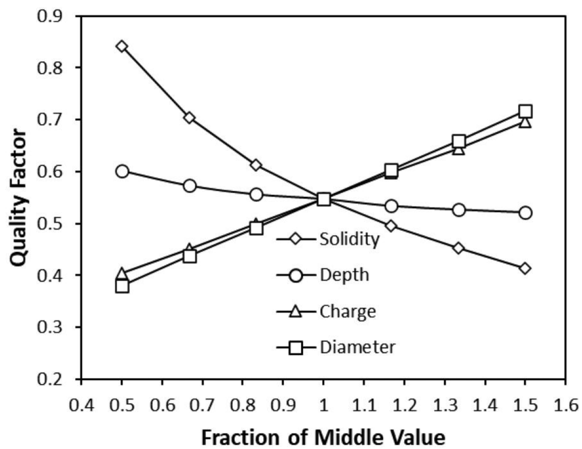

Figure 4. Change in the quality factor relative to fraction of the middle value over the range of values applied to each of the four filter and fiber properties.

value of the four property values, thus producing the same QF value for a fraction of 1.

Fiber charge and diameter had a very similar positive effect on QF with increases across their range of values spanning from QF = 0.38 to 0.71. Fiber charge did not affect filter Δp; therefore, the denominator of Equation 1 remained unchanged as the numerator increased and as efficiency increased (and conversely, penetration decreased), which had an overall positive effect on QF. Conversely, changes in fiber diameter had the largest effect on Δp of all properties across their respective ranges, dropping from 24.2 to 2.7 mm H_2O while all other properties remained at their typical value (Figure S6B). This large decline in Δp due to the inverse-squared effect of fiber diameter more than offsets decreases in efficiency with increases in diameter (Figure S6A) to result in a steady increase in QF with an increase in diameter. However, changes in filter depth caused an increase in both minimum *E* (Figure S4A) and Δp (Figure S4B) that offset each other to result in a negligible decrease in QF from 0.60 to 0.52.

As shown in Figure 4, the lowest value of solidity applied while all other properties remained at their middle value resulted in the highest QF value of 0.84. This condition resulted in the lowest Δp (Figure S5B), which greatly offset the lower efficiency (Figure S5A) obtained under this condition. However, the QF declined with increases in solidity (Figure 4) as the pressure drop increased relatively more than the increase in efficiency.

Constrained filter property optimization

When constraining the filter efficiency to ≥ 95% at the MPPS, the Solver optimization routine in Excel

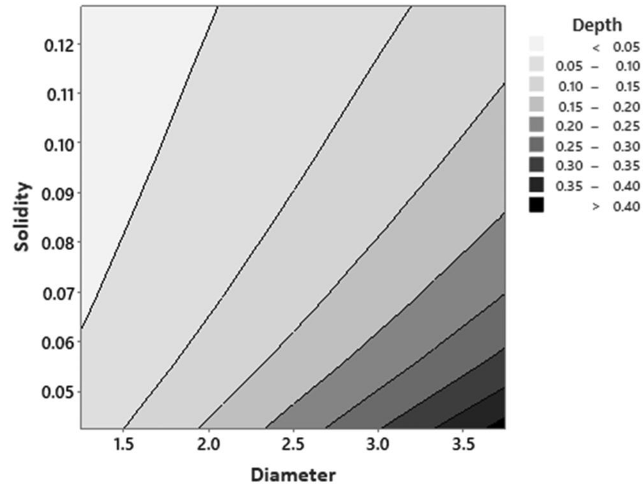

Figure 5. Relationship between fiber diameter (μm), filter solidity, and filter depth (cm) that result in achieving 95% capture efficiency at the most penetrating particle size.

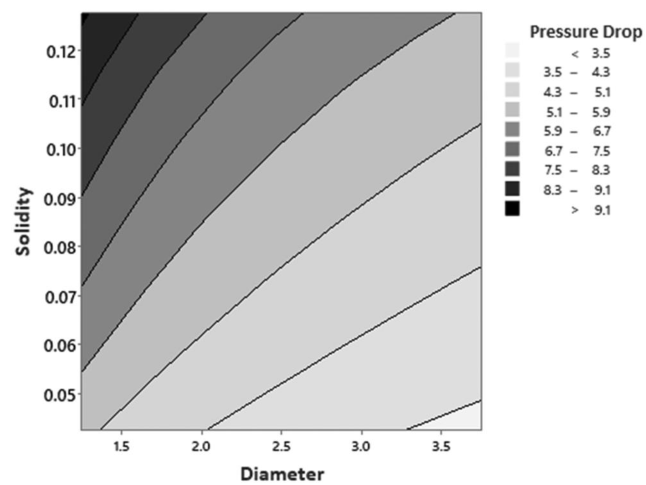

Figure 6. Relationship between fiber diameter (μm), filter solidity, and filter pressure drop (mm H_2O) while achieving 95% capture efficiency at the most penetrating particle size.

provided results that always converged on a minimum filter efficiency at a certain particle diameter of exactly 95%. Therefore, the concept of a quality factor was no longer useful because the numerator of Equation 1 does not change, which left comparisons restricted to conditions that minimize Δp. A contour plot showing the relationship between the three properties that resulted from the optimization procedure is given in Figure 5. The intersection of any two combinations of filter solidity and fiber diameter is in a region of filter depth that satisfies the efficiency criterion. As can be seen in Figure 5, increasingly greater filter depth was required as fiber diameter increased and solidity decreased to meet the criterion.

The Δp values resulting from the optimization routine are shown in Figure 6 in relation to changes in filter solidity and fiber diameter. Although any combination of properties shown in Figure 5 meets the efficiency criterion, Figures 5 and 6 together demonstrate that filters with low solidity, high fiber diameter, and high depth result in producing the lowest Δp, which therefore results in the optimum set of filter properties. However, there is latitude within the ranges of each property, given the results shown in Figure 6, in which even the worst-case combination produced a Δp (9.3 mm H_2O) that is much lower than the NIOSH limit of 35 mm H_2O for inflowing air. Therefore, a reduction from optimal conditions can be afforded to reduce filter thickness and still retain pressure drop at a reasonably low level.

The results shown in Figures 5 and 6 were produced while holding the fiber charge to its typical value of 23.5 μC/m^2. Figure 7 demonstrates the effect of changes in fiber charge on filter depth and pressure drop while satisfying the efficiency criterion. Changes in fiber charge levels could result from different manufacturing methods (Larsen et al. 2021) affecting different filters or, for example, from changes in humidity that affect the charge level of a single filter (Motyl and Łowkis 2006). The plots in Figure 7 were produced while holding the fiber diameter to 2.5 μm. With no charge, both filter depth (Figure 7A) and pressure drop (Figure 7B) markedly increased as expected relative to conditions within the range of charges evaluated in this study. The effect of an increase in filter charge enables thinner filters to meet the efficiency criterion, the effect of which is a lower pressure drop. In effect, Figure 7B displays the transition from thick uncharged filters of the past to the thin charged filters of contemporary N95 FFRs on filter Δp.

As mentioned, using the criterion of ≥ 95% at the MPPS does not accurately relate to the NIOSH approval method that evaluates the efficiency of all particles of the challenge aerosol collectively. The NIOSH test requires the use of a salt aerosol with a lognormal distribution having a geometric mean of 0.075 μm and a geometric standard deviation of 1.80. The relative frequencies of particle diameters having such a distribution were computed for 31 evenly spaced values on a log scale between 0.001 and 1 μm using the equation for a lognormal distribution, which encapsulated >99.99% of the distribution. The model was developed to determine the capture efficiencies at each of the 31 diameters. Solver was then used to repeat the process of determining the filter depth, given a fiber diameter and filter solidity, which caused an overall 95% reduction in the frequency values of the distribution as being proportional to their count values.

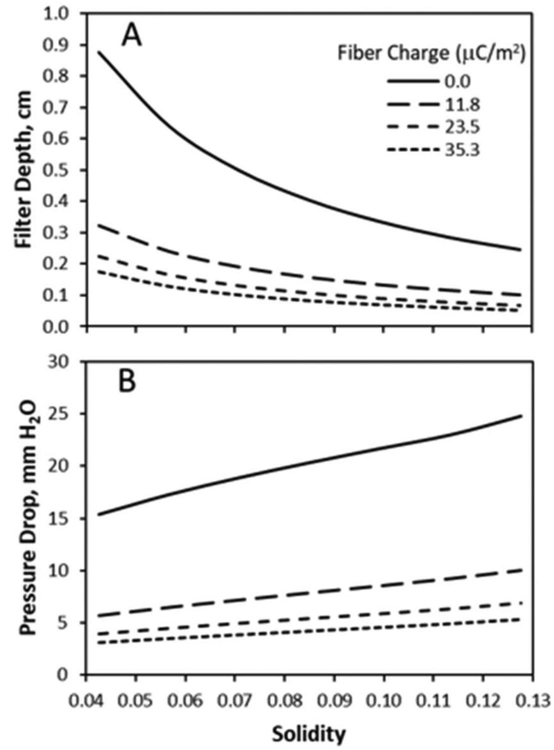

Figure 7. Relationship between filter solidity and filter depth (A) and pressure drop (B) for varying levels of fiber charge while achieving 95% capture efficiency at the most penetrating particle size and with fiber diameter held at 2.50 μm.

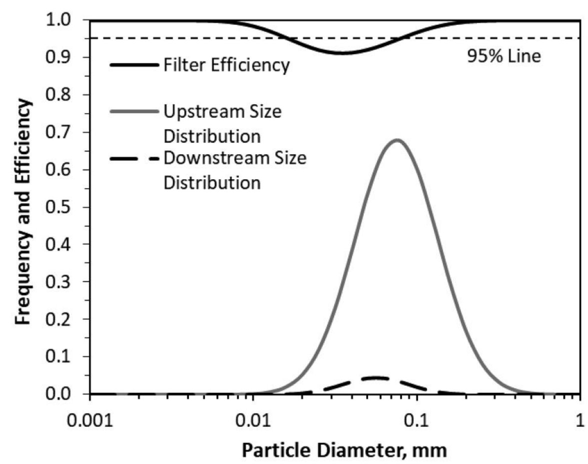

Figure 8. The filter efficiency curve and related upstream and downstream aerosol size distributions resulting when the NIOSH N95 FFR approval test was applied to the model.

An example of the aerosol frequency distribution and resulting total efficiency curve satisfying the NIOSH criterion when all typical property values were applied is given in Figure 8. The efficiency at the MPPS was 91.2%. Such an efficiency of <95% at the MPPS is possible because the test's measure of efficiency is derived from the removal of all particles within the aerosol distribution, which includes those in the tails of the distribution that are captured with >95% efficiency. An analysis of the differences between the NIOSH criterion and the criterion based on the MPPS demonstrated that use of the less restrictive NIOSH criterion resulted in filter depths that met the NIOSH criterion that were 73% to 84% of those using the more stringent criterion based on the MPPS, with commensurate reductions in filter pressure drop.

Filter depth and pressure drop regression models

A GLM to predict the filter depth needed to meet the efficiency criterion based on fiber diameter and filter solidity as independent variables was best developed using the natural logarithm of filter depth as the dependent variable. The GLM was created as a second-order linear model to allow for curvature in the regression model. Likewise, interaction terms were added if found to be significant ($p \leq 0.05$). The resulting coefficients of the GLM are given in Table 3. The model adjusted R-squared value was 0.9990, and all coefficients were significant with p-values < 0.001.

A second GLM to predict Δp with an inflow face velocity of 8 cm/s was developed using Δp in units of mm H2O as the dependent variable and the fiber diameter, filter solidity, and filter depth as the independent variables, where the first GLM was used to obtain the filter depth values. The resulting second-order model with significant interactions had an adjusted R-squared value of 0.9996. All coefficients were significant with p-values < 0.001, except the solidity-squared term, for which $p = 0.005$. The resulting coefficients are given in Table 3. The randomness and normal distribution of the residuals are shown in Figure S8, which demonstrates that the model accounts for all but random variations in pressure drop. However, it is noted that this model is necessarily subject to multicollinearity, given that filter depth is first predicted by fiber diameter and solidity using the optimization routine and then used to predict pressure drop. These models intend to provide a simple method for predicting depth and a resulting pressure drop given known fiber diameter and filter solidity values.

Limitations

There are sources of error in the models used to obtain the results presented in this paper that may cause the GLMs to provide results that deviate from an actual N95 FFR. The first is related to the accuracy of the pressure drop model given in Equations 3 and 4. O'Shaughnessy et al. (2023) produced an adjustment to a filter pressure drop model developed before the advent of contemporary N95 FFRs based on measurements of filter depth, fiber diameter, and solidity of six N95 FFRs, all of which contain uncertainties related to the measurement processes for each. The magnitude of these properties also highly influenced the modeled estimation of total filter efficiency. In particular, fiber diameter is difficult to accurately measure, and the fibers of a filter have a distribution of diameters. O'Shaughnessy et al. (2023) demonstrated that applying a distribution of diameters to the model produced an efficiency curve relative to particle diameter that was more accurate than using the average diameter over the entire dip in efficiency. However, applying a distribution of diameters results in additional model complexity that does not contribute to an accurate prediction of the MPPS, which is nearly identical whether the average diameter or the entire distribution of fiber diameters is applied to the model. Furthermore, the N95 FFR modeled here was treated as having a single layer of filter media, whereas most N95 FFRs have two to three layers, which may add to both the E and Δp of the actual respirator. For example, Purdy (2019) determined that the Δp contributed by the particle filtering layer of 10 N95 FFRs ranged between 61% and 94% of the total Δp.

Table 3. Coefficients and related p-values applied to general linear models to predict filter depth and pressure drop.

Term	ln(Depth) ln(cm)	p-value	Pressure Drop mm H_2O	p-value
Constant	−3.103	<0.001	7.172	<0.001
Diameter	1.400	<0.001	−4.500	<0.001
Solidity	−27.009	<0.001	54.310	<0.001
Depth			−1.934	<0.001
Diameter*Diameter	−0.145	<0.001	2.103	<0.001
Solidity*Solidity	78.750	<0.001	33.500	0.005
Diameter*Solidity			−13.804	<0.001
Diameter*Solidity*Depth			−238.200	<0.001

Conclusion

Two mathematical models were developed previously by this research group in which key aspects of the equations applied were adjusted to best represent the particle capture efficiency (*E*) and pressure drop (Δp) of contemporary N95 FFRs. Those equations were used in this study to determine the combination of filter properties that caused the greatest changes in both outcomes, as well as to determine the set of property conditions that minimizes pressure drop as an optimization goal.

Study results demonstrated that *E* was most influenced by changes in filter solidity and least influenced by fiber charge. Likewise, Δp was most influenced by fiber diameter and least influenced by changes in filter depth. As a relative indication of filter performance that considers the positive effect of more *E* and the negative effect of Δp, an assessment of the quality factor (QF) demonstrated that QF increased with increases in the fiber properties, charge, and diameter, and decreased with increases in the filter properties, solidity, and depth. This study was conducted while using an intuitive approach to filter optimization in which the fiber diameter and filter solidity were assumed to be previously known properties of the filter. Filter depth was then computed for each set of diameter and solidity to minimize Δp while meeting an E criterion of $\geq$ 95% at the most penetrating particle size. When the associated sets of the three properties were then applied to the Δp model, the results indicated that the combination of high fiber diameter, low solidity, and high filter depth produced filters with the lowest pressure drop. There was no localized minimum pressure drop within the ranges of the properties analyzed, suggesting that the primary constraint to developing filters with ever lower pressure drop is the extent to which additional filter thickness can be tolerated in the N95 FFR design. A secondary analysis also demonstrated that increasing fiber charge will diminish the filter depth needed to meet the E criterion, with the consequence of also diminishing Δp.

Acknowledgments

The author would like to thank Zoe Harris, Matthew Purdy, Craig Holder, Raju Ahmed, Joel Ramirez, and Ralph Altmaier for their contributions to the science of respirator filtration theory and practice engaged at the University of Iowa.

Author contributions

CRediT: **Patrick T. O'Shaughnessy**: Conceptualization, Writing – review & editing.

Disclosure statement

No potential conflict of interest was reported by the author.

Funding

This research was supported by the University of Iowa Environmental Health Sciences Research Center (NIH P30 ES005605), and by a pilot project grant from the Heartland Center for Occupational Health and Safety, a NIOSH/CDC Education and Research Center (T42OH008491).

ORCID

Patrick T. O'Shaughnessy http://orcid.org/0000-0001-9173-2722

Data availability statement

All measured and computer-generated data created as part of this research are available from the corresponding author upon request. The N95 FFR filter efficiency model produced as a result of this study, in either Excel or MATLAB, is available from the corresponding author upon request.

References

Balazy A et al. 2006. Manikin-based performance evaluation of N95 filtering-facepiece respirators challenged with nanoparticles. Ann Occup Hyg. 50(3):259–269. https://doi.org/10.1093/annhyg/mei058

Barrett LW, Rousseau AD. 1998. Aerosol loading performance of electret filter media. Am Ind Hyg Assoc J. 59(8):532–539. https://doi.org/10.1080/15428119891010703

Brown RC. 1993. Air filtration: an integrated approach to the theory and applications of fibrous filters. Pergamon Press.

Chen CC, Lehtimaki M, Willeke K. 1993. Loading and filtration characteristics of filtering facepieces. Am Ind Hyg Assoc J. 54(2):51–60. https://doi.org/10.1080/15298669391354324

Davies CN. 1953. The separation of airborne dust and particles. Proc Inst Mech Eng. 167(1b):185–213. https://doi.org/10.1177/002034835316701b13

Davies CN. 1973. Air filtration. Academic Press.

Fylstra D, Lasdon L, Watson J, Waren A. 1998. Design and use of the Microsoft Excel Solver. Interfaces (Providence). 28(5):29–55. https://doi.org/10.1287/inte.28.5.29

Hinds WC. 1999. Aerosol technology: properties, behavior, and measurement of airborne particles. Vol. 2. John Wiley & Sons. Book, Whole.

Huang S-H et al. 2013. Factors affecting filter penetration and quality factor of particulate respirators. Aerosol Air

Qual Res. 13(1):162–171. https://doi.org/10.4209/aaqr.2012.07.0179

Janssen L, Anderson N, Cassidy P, Weber R, Nelson T. 2005. Interpretation of inhalation airflow measurements for respirator design and testing. J-Int Soc Respir Protect. 22(3/4):122.

Kamil AI, Munir MM. 2023. Structure and morphology optimization of nanofiber membrane for the application of high-performance air filtration. Powder Technol. 430: 118978. https://doi.org/10.1016/j.powtec.2023.118978

Larsen GS et al. 2021. Polymer, additives, and processing effects on N95 filter performance. ACS Appl Polym Mater. 3(2):1022–1031. https://doi.org/10.1021/acsapm.0c01294

Lathrache R, Fissan H. 1987. Enhancement of particle deposition in filters due to electrostatic effects. Filtr Separat. 24(6):418–422.

Lee KW, Liu BYH. 1982. Theoretical study of aerosol filtration by fibrous filters. Aerosol Sci Technol. 1(2):147–161. https://doi.org/10.1080/02786828208958584

Motyl E, Łowkis B. 2006. Effect of air humidity on charge decay and lifetime of PP electret nonwovens. Fibres Textiles Eastern Europe. 14(5):39–42.

Napoli NJ, Rodrigues VR, Davenport PW. 2022. Characterizing and modeling breathing dynamics: flow rate, rhythm, period, and frequency. Front Physiol. 12: 772295. https://doi.org/10.3389/fphys.2021.772295

NIOSH. 2019a. Determination of inhalation resistance test, air-purifying respirators standard testing procedure. Report No. TEB-APR-STP-0007, Revision 2.3 ed.

NIOSH. 2019b. Determination of particulate filter efficiency level for N95 series filters against solid particulates for non-powered, air-purifying respirators standard testing procedure. Procedure No. TEB-APR-STP-0059, Revision 3.2 ed.

Niu Z, Bian Y, Xia T, Zhang L, Chen C. 2021. An optimization approach for fabricating electrospun nanofiber air filters with minimized pressure drop for indoor $PM_{2.5}$ control. Build Environ. 188:107449. https://doi.org/10.1016/j.buildenv.2020.107449

O'Shaughnessy P. 2022. Review and demonstration of equations applied to models of filtering facepiece respirator particle capture efficiency. J Occup Environ Hyg. 19(10-11): 615–628. https://doi.org/10.1080/15459624.2022.2112685

O'Shaughnessy P, Harris Z, Purdy M, Altmaier R. 2023. Validation of N95 respirator models for pressure drop and particle capture efficiency. J Occup Environ Hyg. 20(9): 390–400. https://doi.org/10.1080/15459624.2023.2227658

O'Shaughnessy P et al. 2021. Characterization of performance and disinfection resilience of nonwoven filter materials for use in 3D-printed N95 respirators. J Occup Environ Hyg. 18(6):265–275. https://doi.org/10.1080/15459624.2021.1913283

Pradhan AK, Das D, Chattopadhyay R, Singh SN. 2016. An approach of optimal designing of nonwoven air filter media: effect of fibre fineness. J Ind Text. 45(6):1308–1321. https://doi.org/10.1177/1528083714559566

Ptak T. 1993. Optimization of nonwoven filter performance for intermediate Reynolds numbers. Part Sci Technol. 11(3-4):133–145. https://doi.org/10.1080/02726359308906629

Purdy M. 2019. Comparison of facemask characteristics with user assessment of comfort. The University of Iowa.

Ramirez JA, O'Shaughnessy PT. 2016. The effect of simulated air conditions on N95 filtering facepiece respirators performance. J Occup Environ Hyg. 13(7):491–500. https://doi.org/10.1080/15459624.2016.1143950

Stechkina IB, Kirsch AA, Fuchs NA. 1969. Studies on fibrous aerosol filters. IV. Calculation of aerosol deposition in model filters in the range of maximum penetration. Ann Occup Hyg. 12(1):1–8.

Wang J, Chen DR, Pui DYH. 2007. Modeling of filtration efficiency of nanoparticles in standard filter media. J Nanopart Res. 9(1):109–115. https://doi.org/10.1007/s11051-006-9155-9